

Deep subsurface waveguides with circular cross section produced by femtosecond laser writing

V. Diez-Blanco, J. Siegel, A. Ferrer, A. Ruiz de la Cruz, and J. Solis

Citation: *Appl. Phys. Lett.* **91**, 051104 (2007); doi: 10.1063/1.2761298

View online: <http://dx.doi.org/10.1063/1.2761298>

View Table of Contents: <http://apl.aip.org/resource/1/APPLAB/v91/i5>

Published by the [American Institute of Physics](http://www.aip.org).

Related Articles

Compositional nonuniformities in pulsed laser atom probe tomography analysis of compound semiconductors
J. Appl. Phys. **111**, 064908 (2012)

Laser and focused ion beam combined machining for micro dies
Rev. Sci. Instrum. **83**, 02B901 (2012)

Note: Femtosecond laser micromachining of straight and linearly tapered capillary discharge waveguides
Rev. Sci. Instrum. **82**, 096104 (2011)

Study of laser beam propagation in microholes and the effect on femtosecond laser micromachining
J. Appl. Phys. **109**, 123506 (2011)

Invited Article: CO₂ laser production of fused silica fibers for use in interferometric gravitational wave detector mirror suspensions
Rev. Sci. Instrum. **82**, 011301 (2011)

Additional information on *Appl. Phys. Lett.*

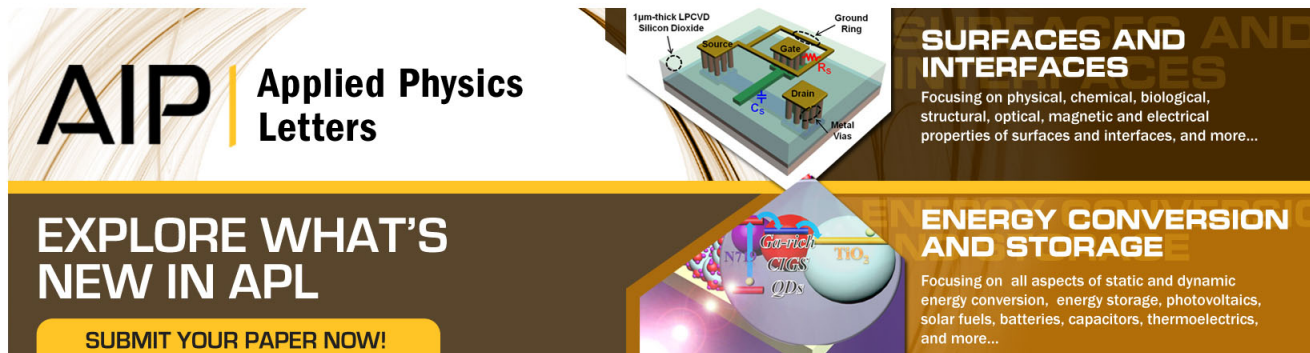
Journal Homepage: <http://apl.aip.org/>

Journal Information: http://apl.aip.org/about/about_the_journal

Top downloads: http://apl.aip.org/features/most_downloaded

Information for Authors: <http://apl.aip.org/authors>

ADVERTISEMENT



AIP Applied Physics Letters

EXPLORE WHAT'S NEW IN APL

SUBMIT YOUR PAPER NOW!

SURFACES AND INTERFACES
Focusing on physical, chemical, biological, structural, optical, magnetic and electrical properties of surfaces and interfaces, and more...

ENERGY CONVERSION AND STORAGE
Focusing on all aspects of static and dynamic energy conversion, energy storage, photovoltaics, solar fuels, batteries, capacitors, thermoelectrics, and more...

The advertisement features a central graphic with a 3D schematic of a device on a substrate, labeled with '1µm-thick LPCVD Silicon Dioxide', 'Source', 'Gate', 'Drain', 'Metal Vias', and 'Ground Ring'. Below this, there are smaller images showing a quantum dot (QD) and a molecular structure with 'NO₂' and 'C₆₀' labels.

Deep subsurface waveguides with circular cross section produced by femtosecond laser writing

V. Diez-Blanco, J. Siegel, A. Ferrer, A. Ruiz de la Cruz, and J. Solis^{a)}

Laser Processing Group, Instituto de Optica, CSIC, Serrano 121, 28006 Madrid, Spain

(Received 28 March 2007; accepted 28 June 2007; published online 31 July 2007)

A combination of low numerical aperture focusing optics, in order to minimize spherical aberration, and beam shaping with a slit has been used to produce waveguides in fused silica by femtosecond laser writing. Waveguides with circular cross section and low losses are produced over a large depth window (>7 mm) without changing any experimental parameter. Diffraction induces beam divergence along the axis perpendicular to the slit, leading to a shift of the focal plane. The focal intensity distribution can be predicted by a hybrid model combining Gaussian beam propagation with imaging of the slit into the material. © 2007 American Institute of Physics.

[DOI: 10.1063/1.2761298]

Nonlinear processing of dielectric materials with femtosecond laser pulses is a very promising tool for the fabrication of three-dimensional photonic elements.¹ However, in spite of its application to the production of waveguides,² couplers,³ waveguide amplifiers,⁴ or lasers,⁵ its use is still limited by several problems affecting the spatial distribution of energy deposited inside the dielectric material. Spherical aberration (SA), caused by the refractive index mismatch at the air-dielectric interface,⁶⁻⁹ as well as nonlinear propagation (NLP) phenomena¹⁰⁻¹² have already been identified as critical issues in this respect. Depth of focus limitations, SA, and NLP can result in an elongated focal volume, leading to structures with a strongly elliptical cross section.

In the absence of NLP and SA effects, the extension (ΔZ) of the focal volume along the beam propagation axis (z) is given by twice the Rayleigh range (Z_R) of the beam:¹³ $\Delta Z = 2Z_R = 2n\lambda / \pi(\text{NA})^2$, n being the refractive index of the material, λ the laser wavelength, and NA the numerical aperture of the focusing lens. The transverse dimension of the beam at the focus is given by $2w_{0,xy} = 2\lambda / \pi(\text{NA})$, where $w_{0,x}$ ($w_{0,y}$) denotes the $1/e^2$ intensity radius at the focus along the x (y) axis. As a consequence, the focal volume is a prolate ellipsoid with an aspect ratio $Z_R/w_{0,x}$ equal to n/NA . High NA optics ($\text{NA} > 1$) thus allows generating a quasispherical focal volume at very shallow processing depths in low refractive index materials.¹⁴ However, the focal volume size can be then too small for applications, such as the production of IR transmitting waveguides, making it necessary the use of high repetition rate laser systems to increase the size of the laser modified volume through thermal diffusion effects.^{14,15}

SA can also strongly contribute to ΔZ , particularly for large values of NA and focusing depths d .⁷ A geometrical estimation for this contribution is given by⁸

$$\Delta z_{\text{SA}} \approx d \left(\sqrt{\frac{1 - (\text{NA}/n)^2}{1 - \text{NA}^2}} - 1 \right). \quad (1)$$

The problem of obtaining small ΔZ values that are comparable to the beam waist ($2w_0$) is illustrated in Fig. 1. It shows the calculated intensity distribution⁶ along the yz plane for a ($\lambda = 800$ nm) laser beam focused at $d = 1$ mm in-

side a material with $n = 1.45$, for different NA values. For low NAs (0.1 and 0.2), ΔZ is essentially given by the Rayleigh range. A further increase of the NA ($\text{NA} = 0.6$) makes the SA contribution to dominate leading to an elongated filament. This behavior can be quantitatively appreciated in the plot in Fig. 1, showing $2Z_R$, ΔZ_{SA} , $2Z_R + \Delta Z_{\text{SA}}$, and $2w_0$ as a function of NA. The minimum observed in $2Z_R + \Delta Z_{\text{SA}}$ for $\text{NA} \sim 0.2$ corresponds to the window over which the best compromise can be achieved. This compromise is though far from generating a focal volume with a circular cross section. For the parameters used, at $d = 1$ mm, ΔZ is around $20 \mu\text{m}$ while $2w_0$ is just about $2.5 \mu\text{m}$. For shallower depths, e.g., $d = 0.3$ mm, the best compromise would be found at $\text{NA} \sim 0.3$, with $\Delta Z \sim 10 \mu\text{m}$ and $2w_0 \sim 1.7 \mu\text{m}$. For larger depths, e.g., $d = 10$ mm, the minimum of ΔZ ($\sim 80 \mu\text{m}$) would be centered on $\text{NA} = 0.11$.

For the particular case of waveguides, the use of elliptically shaped beams¹⁶⁻¹⁹ provides an alternative route for producing elements with circular cross section. The smaller transverse dimension of the elliptical beam gets less focused and can reach a size ($2w_{0,y}$) comparable to $2Z_R$, thus generating a focal volume shaped as a thin disk.¹⁶ If the sample is translated along the direction perpendicular to the disk during the writing process, the resulting waveguide shows a nearly circular cross section.^{16,18} So far, this approach has been used only for shallow processing depths (negligible SA). In this work we have used a combination of two complementary approaches (use of a small NA for minimizing SA and elliptical beam shaping) to achieve the produc-

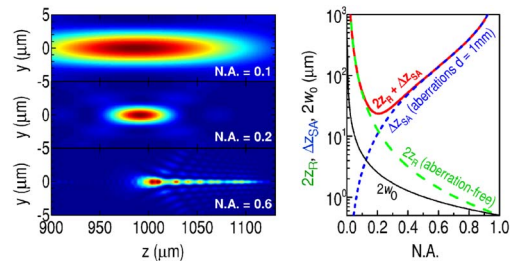


FIG. 1. (Color online) Intensity distribution in the yz plane (z is the propagation axis) of a $\lambda = 800$ nm laser beam focused at $d = 1$ mm inside fused silica, calculated for $\text{NA} = 0.1, 0.2$, and 0.6 . The plot shows the evolution of $2Z_R$, Z_{SA} , $2Z_R + Z_{\text{SA}}$, and $2w_0$ as a function of NA computed under the same conditions for n , λ , and d .

^{a)}Electronic mail: j.solis@io.cfmac.csic.es

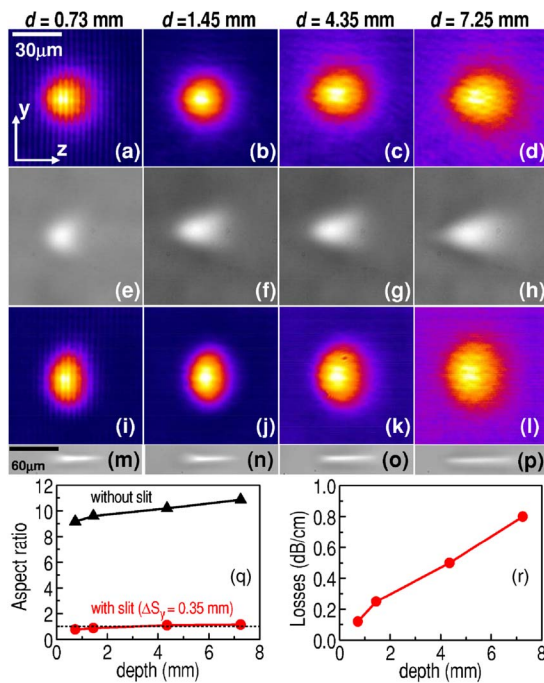


FIG. 2. (Color online) [(a)–(d) and (i)–(l)] Images of the guided modes at 633 nm at the exit face of waveguides produced at the indicated writing depths d . The slit width and pulse energy used was $\Delta S_y = 0.35$ mm and $E = 4$ μJ for (a)–(d) and $\Delta S_y = 0.25$ mm and $E = 8$ μJ for (i)–(l). [(e)–(h) and (m)–(p)] Transillumination images of structures produced at the same depths with slit [(e)–(h)] $\Delta S_y = 0.35$ mm and $E = 4$ μJ and without slit ($E = 1$ μJ). (q) Aspect ratio of the waveguides/structures produced with a slit ($\Delta S_y = 0.35$ mm and $E = 5.6$ μJ) and without a slit ($E = 1$ μJ). The dotted line indicates the ideal aspect ratio of 1. (r) Propagation losses at 1550 nm as a function of depth ($\Delta S_y = 0.25$ mm and $E = 8$ μJ).

tion of optical waveguides with circular cross sections over a large processing depth window (beyond 7 mm).

The samples, (Schott-Lithosil) fused silica blocks, were irradiated using 100 fs laser pulses delivered by a commercial Ti:Al₂O₃ amplifier ($\lambda = 800$ nm and a repetition rate of 1 kHz). The writing beam (parallel to the z axis) was focused at different depths in the 0.7–7 mm range inside a $2 \times 2 \times 1$ cm³ fused silica block using a long working distance microscope objective with a focal length $f = 20$ mm, a nominal NA of 0.26, and a working distance of 30 mm. During irradiation, the sample was scanned along the x axis (perpendicularly to the irradiation beam) at 100 $\mu\text{m/s}$ generating waveguides with a length of ~ 2 cm. The $1/e^2$ intensity beam diameter along the x axis at the entrance of the focusing optics was $D_x = 7.43$ mm, corresponding to an effective numerical aperture $\text{NA}_x = 0.18$. An adjustable slit located 210 mm before the focusing optics was used to reduce the effective numerical aperture of the beam along the y axis (NA_y). The effect of the slit width (ΔS_y), the writing depth (d), and the writing pulse energy (E) on the characteristics of the produced waveguides was studied. Details regarding the setup used for characterizing the waveguides are given elsewhere.¹¹ The propagation losses and refractive index change of the waveguides were measured using the methods described in Refs. 20 and 21, respectively.

The first and third rows of images in Fig. 2 show the near field intensity distribution of the guided mode at 633 nm of two groups of waveguides. Each group corresponds to four different irradiation depths for a given slit width (ΔS_y) and pulse energy (E). The first row corresponds

to the waveguides with the most circular mode cross section obtained in this study, corresponding to $\Delta S_y = 0.35$ mm. Circularity is achieved at the already considerable depth of 0.73 mm and maintained up to the largest depth explored ($d = 7.25$ mm). The second row shows white light transillumination images corresponding to these waveguides. Although their shape is slightly elongated, particularly at large depths, their nearly circular size and aspect ratio are consistent with the one observed in the images of the guided modes. In general, for values of ΔS_y in the 0.20–0.50 mm range, the guided modes show an aspect ratio $\text{AR} = (D_z/D_y)$ close to 1 (D_z and D_y denote the full width at half maximum of the intensity distribution of the mode along the y and z axes, respectively) while the refractive change of the waveguides shows values typically around $\Delta n \sim 5 \times 10^{-4}$.

The diameters of the waveguides (average of vertical and horizontal dimensions) have been determined from the transillumination images, providing a full width at half maximum values of 14 and 20 μm for depths of 0.73 and 7.25 mm, respectively. Using a higher NA lens, the diameter can be decreased further at the expense of the maximum working depth. We have estimated that using a NA of 0.3 circular waveguide diameters below 10 μm can be produced for depths up to 2 mm. For larger depths, adaptive optics²² can be used to minimize the SA effects.

It is even possible to obtain a stronger elongation along the y axis by sufficiently reducing the slit width, as evident in the third row of Fig. 2. For comparison we have also included in the fourth row of Fig. 2 a set of white light transillumination images of regions modified by a circular beam (aperture fully opened). The produced structures do not support a guided mode at 633 nm. The images correspond to the same experimental conditions used for the first and third rows but with a lower energy (1 μJ) to account for the smaller focal volume and to suppress any possible NLP contribution. The scale of these images is twice the one used in the images [(a)–(l)] in the same figure. For $d = 7.25$ mm, $\Delta Z \sim 90$ μm , which is in excellent agreement with the value expected from Eq. (1) for a $\text{NA}_{x,y} = 0.18$. The value corresponding to $\Delta S_y = 0.35$ mm for the shallowest depth shown, $d = 0.73$ mm, is just about one-third of this value (~ 30 μm) leading a circular aspect ratio. According to Ref. 18, in order to produce a circular disk-shaped focal volume working at shallow depths, the ratio between the shorter and the longer beam axes at the entrance of the focusing optics would be $R_x/R_y = [(n/\text{NA})\sqrt{(3/\ln 2)}]$. For our effective numerical aperture ($\text{NA} \approx 0.18$) these should lead to an optimal value for $R_x/R_y \sim 20$. We obtain the best waveguides in terms of aspect ratio for values $R_x/R_y \approx 21$, in excellent agreement with the estimation. The most important difference is that in our case the circular cross section is maintained for depths ten times deeper (beyond 7 mm). This is further illustrated in the left plot of Fig. 2, where we have plotted AR as a function of the processing depth both for $\Delta S_y = 0.35$ and for the structures induced with the slit fully open. It can be clearly seen that in the first case AR remains close to 1, no matter the value of d , while for the “slitless” structures, $\text{AR} > 9$. The evolution of the propagation losses of the waveguides at 1550 nm as a function d is also shown in the right plot of Fig. 2. While losses as low as 0.2 dB/cm can be obtained at $d = 0.72$ mm, they are kept < 1 dB/cm at depths beyond 7 mm.

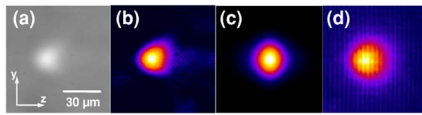


FIG. 3. (Color online) (a) Gray and (b) pseudocolor scale transillumination images of a waveguide written at $d=0.73$ mm and $E=4$ μ J and a slit width of 0.35 mm. In (b) the contrast of the image has been enhanced by subtracting the level of the homogenous background of the image. (c) Calculation of the intensity distribution produced by the writing laser in the focal region for the corresponding slit width. The distribution has been obtained from the hybrid model of Gaussian beam propagation and slit aperture imaging and by then applying a I^2 scaling to account for the nonlinear absorption of the laser light in fused silica. (d) Pseudocolor scale image of the guided mode at 633 corresponding to images (a) and (b).

In absence of SA and NLP, the spatial intensity distribution for an elliptical beam focused from air inside a material with refractive index n is given by

$$I(x, y, z) \propto \frac{\exp\{-2[(x^2/w_x^2(z)) + (y^2/w_y^2(z))]\}}{\sqrt{1 + ((z/z_{R_x})^2) \times \sqrt{1 + [(z - z_0)/z_{R_y}]^2}}, \quad (2)$$

where $z=0$ corresponds to the focal plane, $w_x(z)=w_{0_x}(1 + (z/z_{R_x})^2)^{1/2}$, $w_{0_x}=2\lambda f/\pi R_x$, $Z_{R_x}=n\lambda f^2/\pi R_x^2$, and R_x denotes the $1/e^2$ intensity beam radius at the focusing lens along the x axis (corresponding expressions apply for the y axis). The two Rayleigh ranges (Z_{R_x} and Z_{R_y}) are independent and z_0 denotes the difference in the z coordinate of the beam waist position over the xz and yz planes. In our case this offset is motivated by the fact that the beam diffracted at the aperture is not collimated in the yz plane and thus shows a noninfinite radius of curvature (ρ_y) after the slit. Using the $ABCD$ matrix formalism for the propagation of a Gaussian beam¹³ it is possible to compute the values for z_0 and w_{0_y} from the experimental values of λ , n , f , R_y , and ρ_y . We have used this approach to calculate the intensity distribution in the focal region for different slit width values using Eq. (2). The shape of the distributions obtained is though far from reproducing the shape of the intensity cross sections of the waveguides. The reason for this discrepancy is clearly related to the fact that we are not dealing with a real Gaussian elliptical beam but with a beam shaped by a hard aperture and diffraction.

In order to compute this effect we have developed a hybrid model to calculate the intensity distribution at the focus. The model is based in the assumption that the focusing lens is forming an image of the aperture and the position and size of the beam waist in the yz plane are thus calculated by using geometrical optics. The so-calculated values of z_0 and w_{0_y} are then used along with the corresponding values for the xz plane, given by the above expressions for a collimated Gaussian beam, to calculate the intensity distribution using Eq. (2). In order to account for the nonlinear absorption process in the glass, the calculated intensity distributions have been elevated to the fifth power, corresponding to a five photon nonlinear absorption process at a wavelength of 800 nm and experimentally measured band gap of 7.1 eV. The results are shown in Fig. 3. The agreement between calculation [Fig. 3(c)] and the experimental transillumination [Figs. 3(a) and 3(b)] and guided mode [Fig. 3(d)] images can be considered excellent both in terms of shape and size of the structures. The result is particularly remarkable considering the relative simplicity of the model used.

In summary we have shown that a combination of low NA optics along with the use of beam shaping allows producing waveguides with circular cross sections at large processing depths. The aspect ratio of the guided mode is found to be essentially independent of the pulse energy over a depth processing window of more than 7 mm, while losses can be maintained below 1 dB/cm. Finally, the presence of diffraction at the slit aperture generates a shift between the xz - and yz -focal planes. This shift and the size of the transformed region inside the material can be predicted by using a hybrid model for calculating the intensity distribution in the focal region.

This work has been partially supported by the Spanish Ministry of Education through TEC 2005-00074 project and by the EU in the frame of the TMR project "FLASH" (MRTN-CT-2003-503641). One of the authors (V.D.-B.) acknowledges the financial support of the CSIC and the European Social fund through an I3P Ph.D. fellowship. The authors acknowledge J. Portilla and C. Dorrnsoro for their help in programing the hybrid model.

¹K. Hirao, T. Mitsuyu, J. Si, and J. Qiu, *Active Glass for Photonic Applications: Photoinduced Structures and their Application*, Springer Series on Photonics (Springer, Berlin, 2001), Vol. 7.

²K. M. Davis, K. Miura, N. Sugimoto, and K. Hirao, *Opt. Lett.* **21**, 1729 (1996).

³K. Minoshima, A. Kowalevicz, I. Hartl, E. P. Ippen, and J. G. Fujimoto, *Opt. Lett.* **26**, 1516 (2001).

⁴Y. Sikorski, A. A. Said, P. Bado, R. Maynard, C. Florea, and K. A. Winick, *Electron. Lett.* **36**, 226 (2000).

⁵S. Taccheo, G. Della Valle, R. Osellame, G. Cerullo, N. Chiodo, P. Laporta, O. Svelto, A. Kili, U. Morgner, M. Lederer, and D. Kopf, *Opt. Lett.* **29**, 2626 (2004).

⁶A. Marcinkevicius, V. Mizeikis, S. Joudkazis, S. Matsuo, and H. Misawa, *Appl. Phys. A: Mater. Sci. Process.* **76**, 257 (2003).

⁷C. Hnatovsky, R. S. Taylor, E. Simova, V. R. Bhardwaj, D. M. Rayner, and P. B. Corkum, *J. Appl. Phys.* **98**, 013517 (2005).

⁸Q. Sun, H. Jiang, Y. Liu, Y. Zhou, H. Yang, and Q. Gong, *J. Opt. A, Pure Appl. Opt.* **7**, 655 (2005).

⁹D. Liu, Y. Li, R. An, Y. Dou, H. Yang, and Q. Gong, *Appl. Phys. A: Mater. Sci. Process.* **84**, 257 (2006).

¹⁰H. R. Lange, G. Grillon, J. F. Ripoche, M. A. Franco, B. Lamouroux, B. S. Prade, A. Mysyrowicz, E. T. Nibbering, and A. Chiron, *Opt. Lett.* **23**, 120 (1998).

¹¹J. Siegel, J. M. Fernandez-Navarro, A. Garcia-Navarro, V. Diez-Blanco, O. Sanz, J. Solis, F. Vega, and J. Armengol, *Appl. Phys. Lett.* **86**, 121109 (2005).

¹²V. Kudriasov, E. Gaizauskas, and V. Sirutkaitis, *J. Opt. Soc. Am. B* **22**, 2619 (2005).

¹³A. Yariv, *Quantum Electronics in Modern Communications* Oxford Series in Electrical and Computer Engineering (Oxford University Press, New York, 1997), Chap. 2, pp. 39–76.

¹⁴C. B. Schaffer, A. Brodeur, J. F. García, and E. Mazur, *Opt. Lett.* **26**, 93 (2001).

¹⁵R. R. Gattass, L. R. Cerami, and E. Mazur, *Opt. Express* **14**, 5279 (2006).

¹⁶G. Cerullo, R. Osellame, S. Taccheo, M. Marangoni, D. Polli, R. Ramponi, P. Laporta, and S. De Silvestri, *Opt. Lett.* **27**, 1938 (2002).

¹⁷R. Osellame, S. Taccheo, M. Marangoni, R. Ramponi, P. Laporta, D. Polli, S. de Silvestri, and G. Cerullo, *J. Opt. Soc. Am. B* **20**, 1559 (2003).

¹⁸M. Ams, G. D. Marshall, D. J. Spence, and M. J. Withford, *Opt. Express* **13**, 5676 (2005).

¹⁹S. Sowa, W. Watanabe, T. Tamaki, J. Nishii, and K. Itoh, *Opt. Express* **14**, 291 (2006).

²⁰V. Apostolopoulos, L. Laversenne, T. Colomb, C. Depeursinge, R. P. Salathé, M. Pollnau, R. Osellame, G. Cerullo, and P. Laporta, *Appl. Phys. Lett.* **85**, 1122 (2004).

²¹D. Homoelle, S. Wielandy, A. L. Gaeta, N. F. Borrelli, and C. Smith, *Opt. Lett.* **24**, 1311 (1999).

²²M. A. A. Neil, R. Juskaitis, M. J. Booth, T. Wilson, T. Tanaka, and S. Kawata, *Appl. Opt.* **41**, 1374 (2002).